Optimal algorithm of SAR raw data processing for radar cross section estimation

Volodymyr Pavlikov[1,†], Valerii Volosyuk[1,†], Simeon Zhyla[1,†], Kostiantyn Dergachov[1,†], Olena Havrylenko[1,†], Yuliya Averyanova[2,†], Anatoliy Popov[1,†], Ivan Ostroumov[2,*,†], Nikolay Ruzhentsev[1,†], Eduard Tserne[1,†], Tatyana Nikitina[3,†], Oleksandr Shmatko[1,†], Nataliia Kuzmenko[2,†], Olha Sushchenko[2,†], Maksym Zaliskyi[2,†], Oleksandr Solomentsev[2,†] and Borys Kuznetsov[4,†]

[1]National Aerospace University H.E. Zhukovsky "Kharkiv Aviation Institute", Vadym Manko Str., 17, Kharkiv, 61070, Ukraine
[2]State University "Kyiv Aviation Institute", Liubomyra Huzara Ave., 1, Kyiv, 03058, Ukraine
[3]V.N. Karazin Kharkiv National University, Svobody Sq., 4, Kharkiv, 61022, Ukraine
[4]Anatolii Pidhornyi Institute of Power Machines and Systems of the National Academy of Sciences of Ukraine, Komunalnykiv Str., 2/10, Kharkiv, 61046, Ukraine

Abstract

Synthetic aperture radar (SAR) systems are pivotal in remote sensing, offering high-resolution imaging capabilities under diverse environmental conditions. This study introduces an optimal algorithm for SAR raw data processing, addressing the stochastic nature of surface scattering. By modeling the complex scattering coefficient as a random spatial process it is propose a statistically optimized signal processing framework. A key innovation is the incorporation of a decorrelation operation, which increases statistically independent samples, mitigates speckle noise, and enhances image quality. Simulation results demonstrate superior performance over conventional methods across multiple image quality metrics. The proposed algorithm improves radar cross section estimation, offering enhanced resolution and clarity for complex surfaces. This advancement holds significant potential for applications in Earth observation, geohazard monitoring, and structural analysis.

Keywords

synthetic aperture radar, stochastic scattering, decorrelation processing, speckle noise reduction, radar cross section,

1. Introduction

Aerospace, navigation, and remote sensing applications require compact, high-resolution imaging capabilities that can be provided by Synthetic Aperture Radar (SAR) systems [1, 2, 3]. Among the many remote sensing technologies available today, SAR stands out as the most superior because it can provide Earth surface images with resolutions better than one meter [4, 5] at any time of the day or night and in all types of weather conditions. These features make SAR critical for many uses like watching the

CMSE'25: International Workshop on Computational Methods in Systems Engineering, June 12, 2025, Kyiv, Ukraine
*Corresponding author.
†These authors contributed equally.
v.pavlikov@khai.edu (V. Pavlikov); v.volosyuk@khai.edu (V. Volosyuk); s.zhyla@khai.edu (S. Zhyla); k.dergachov@khai.edu (K. Dergachov); o.havrylenko@khai.edu (O. Havrylenko); ayua@kai.edu.ua (Y. Averyanova); a.v.popov@khai.edu (A. Popov); ostroumov@ukr.net (I. Ostroumov); nvruzh@gmail.com (N. Ruzhentsev); e.tserne@khai.edu (E. Tserne); tatjana55555@gmail.com (T. Nikitina); o.shmatko@khai.edu (O. Shmatko); nataliiakuzmenko@ukr.net (N. Kuzmenko); sushoa@ukr.net (O. Sushchenko); maximus2812@ukr.net (M. Zaliskyi); avsolomentsev@ukr.net (O. Solomentsev); kuznetsov.boris.i@gmail.com (B. Kuznetsov)
https://www.ostroumov.sciary.com/ (I. Ostroumov)
0000-0002-6370-1758 (V. Pavlikov); 0000-0002-1442-6235 (V. Volosyuk); 0000-0003-2989-8988 (S. Zhyla); 0000-0002-6939-3100 (K. Dergachov); 0000-0001-5227-9742 (O. Havrylenko); 0000-0002-9677-0805 (Y. Averyanova); 0000-0003-0715-3870 (A. Popov); 0000-0003-2510-9312 (I. Ostroumov); 0000-0003-3023-4927 (N. Ruzhentsev); 0000-0003-0709-2238 (E. Tserne); 0000-0002-9826-1123 (T. Nikitina); 0000-0002-3236-0735 (O. Shmatko); 0000-0002-1482-601X (N. Kuzmenko); 0000-0002-8837-1521 (O. Sushchenko); 0000-0002-1535-4384 (M. Zaliskyi); 0000-0002-3214-6384 (O. Solomentsev); 0000-0002-1100-095X (B. Kuznetsov)

Earth [6], tracking ships [7], finding illegal boats, making digital elevation maps, keeping an eye on geohazards, and checking structures without causing damage.

Radar imaging of various objects, surfaces, subsurface soil layers, atmospheric inhomogeneities, and other natural media requires their mathematical, deterministic, and statistical description, along with the justification of corresponding concepts and definitions. Correct mathematical model of radiated or scattered electromagnetic fields is critical for optimizing the signal processing algorithm and designing the architecture of remote sensing radar systems [8, 9].

Solving the problem of radar imaging for surfaces with small roughness, two-scale surfaces, or complex real-world terrains like forests, grass, or agricultural land is challenging due to the complexity and ambiguity of analytical expressions derived from fundamental diffraction principles such as the Kirchhoff theorem, Rayleigh-Sommerfeld theorem, and Stratton-Chu formulas. Accurate electrodynamic calculations for such surfaces are often infeasible, making a phenomenological approach more practical for determining scattered electromagnetic fields [10]. Typically, radar images are understood as the spatial distribution of a surface's complex scattering coefficient, calculated using Maxwell's equations, wave equations, and corresponding integral equations under specified boundary conditions. However, defining these conditions precisely for many surfaces, especially vegetation, is nearly impossible due to the intricate internal structure of the scattering coefficient. A phenomenological approach, combined with stochastic modeling of electromagnetic fields, is better suited for analyzing coherent images of real-world surfaces.

Despite significant advancements in SAR technology, achieving optimal signal processing under stochastic reflections remains challenging. A critical review of the literature reveals that many radar imaging studies fail to account for the stochastic nature of complex reflection coefficients, favoring deterministic models that oversimplify scattering as a function of spatial coordinates rather than a random process influenced by surface texture, microstructure, and material composition. This simplification limits the application of statistical optimization techniques, such as correlation-aware filter synthesis, leaving unresolved fundamental issues like determining inverse correlation functions essential for optimal estimators in random process theory, ultimately compromising algorithmic performance, particularly in high-noise conditions or varying observation geometries.

In this study, we propose a novel approach that justifies describing the primary coherent image either as a complex Wiener process or as its derivative, represented by non-stationary spatial complex white noise, with its power spectral density governed by the variation in the radar cross section. This approach is underpinned by a statistical framework for signal processing that accounts for the stochastic nature of surface reflections and the internal noise of the radar system. A key element of our proposal is the introduction of a decorrelation operation, which increases the number of statistically independent signal samples, mitigates speckle noise, and substantially improves image quality.

2. Concept of radar image model

A radar image is a complex construct, both in terms of its structural analysis and mathematical representation. Radar imaging can be broadly categorized into two types: coherent and incoherent. Incoherent images are the average intensity of electromagnetic wave without retaining any phase data. On the other hand, coherent imagery depends on the phase information of waves reflected from observed objects. Incoherent radar images are generated by non-coherent radar systems that transmit signals with randomized initial phases. Conversely, SAR systems produce coherent images by processing both the amplitude and phase of received signals. As a result, SAR is classified as a coherent radar technology.

Every separate point in coherent radar image has coordinate (x, y) and represent one elementary scattering area $\Delta S = \Delta x \Delta y$ on the surface. Prior to radar signal processing, wave scattering should be analysed for a surface element of infinitesimal (but finite) area $d\vec{r} = dxdy$. These elements, treated as differential areas during integration, are associated with a scattering (reflection) coefficient:

$$d\dot{Q}(\vec{r}) = \frac{d\dot{E}_{sc}(\vec{r})}{E_0(\vec{r})} \tag{1}$$

where $E_0(\vec{r})$ is the incident electromagnetic field, $d\dot{E}_{sc}(\vec{r})$ is the scattered electromagnetic field by element of the underlying surface.

In radar measurements of the surface, it is not appropriate to talk about the reflection of an infinitely small point, therefore the concept of specific scattering coefficient is introduced

$$\dot{F}(\vec{r}) = \frac{d\dot{Q}(\vec{r})}{d\vec{r}}, \tag{2}$$

$$d\dot{Q}(\vec{r}) = \dot{F}(\vec{r})d\vec{r}, d\dot{E}_{sc}(\vec{r}) = E_0(\vec{r})\dot{F}(\vec{r})d\vec{r}. \tag{3}$$

In many studies [11], this $\dot{F}(\vec{r})$ represents an idealized complex radar image that must be reconstructed through spatiotemporal processing of ground-reflected signals. The electromagnetic field in the antenna aperture region, generated by this specific scattering coefficient $\dot{F}(\vec{r})$, can be characterized using the following theoretical formulations and mathematical expressions:

1. Kirchhoff's integral theorem and scalar theory of diffraction

$$\int_V (\varphi\nabla^2 E - E\nabla^2\varphi)dV = \int_D \left(\varphi\frac{\partial E}{\partial\vec{n}} - E\frac{\partial\varphi}{\partial\vec{n}}\right)dD, \tag{4}$$

   where φ and E are arbitrary continuous complex functions of spatial coordinates with continuous first and second partial derivatives inside the volume V and on the closed surface D enclosing the volume,$\vec{n}$ is the outer normal to the surface D, ∇ is the Hamiltonian operator, ∇^2 is the Laplace operator;

2. Helmholtz-Kirchhoff theorem

$$\dot{E}(\vec{r}') = \frac{1}{4\pi}\int_D \left\{\frac{\partial\dot{E}(\vec{r})}{\partial n}\frac{exp(jkR_D)}{R_D} - \dot{E}(\vec{r})\frac{\partial}{\partial n}\left[\frac{exp(jkR_D)}{R_D}\right]\right\}d\vec{r}, \tag{5}$$

   where $\dot{E}(\vec{r}')$ is the electric field strength in the antenna aperture region with coordinate $\vec{r}'$, $\frac{exp(jkR_D)}{R_D}$ is the Green's function, $k = \frac{2\pi}{\lambda}$ is the wave number, j is the imaginary unit, $\dot{E}(\vec{r}) = E_0(\vec{r})\dot{F}(\vec{r})$ are values of the field's complex amplitudes on the surface D, R_D is the distance to every point on the surface with coordinates $\vec{r}$;

3. Rayleigh-Sommerfeld theory

$$\dot{E}(\vec{r}') = (j\lambda)^{-1}\int_{D_{hole}} \dot{E}(\vec{r})cos(\vec{n},\vec{R})\frac{exp(jkR_D)}{R_D}d\vec{r}, \tag{6}$$

   where D_{hole} is the hole on a flat opaque screen with coordinates $\vec{r} \in D_{hole}$;

4. Stratton-Chu formulas

$$\vec{\dot{E}}(\vec{r}') = -(4\pi)^{-1}Dj0[nH(r)](R) - [[nE(r)]grad(R)] - (nE(r))grad(R)dr, \tag{7}$$

$$\vec{\dot{H}}(\vec{r}') = -(4\pi)^{-1}Dj0[nH(r)](R) + [[nH(r)]grad(R)] + (nH(r))grad(R)dr, \tag{8}$$

   where $\vec{\dot{H}}(\vec{r}')$ is the magnetic field strength.

The fundamental diffraction theories presented here are largely similar, and the choice of which formula to apply in practice depends on experimental conditions and analytical feasibility. To unify these principles of diffraction theory, we propose a phenomenological description of the electromagnetic fields [12, 13, 14]

$$\dot{E}(\vec{r}') = \int_D E_0(\vec{r})\dot{F}(\vec{r})\frac{exp(jkR(\vec{r},\vec{r}'))}{R(\vec{r},\vec{r}')}d\vec{r}, \tag{9}$$

where $R(\vec{r},\vec{r}')$ is a distance from point on the surface with coordinate $\vec{r}$ to the point of antenna surface with coordinate $\vec{r}'$.

After processing the field in the antenna information signal in the receiver can be represented in a simplified form [15, 16] :

$$s_r(t) = Re\left\{\int_D \dot{F}(\vec{r})\dot{s}_0(t,\vec{r})d\vec{r}\right\} = Re\left\{\int_D \dot{s}_0(t,\vec{r})d\dot{Q}(\vec{r})\right\}, \tag{10}$$

where $\dot{s}_0(t,\vec{r})$ is the reference signal for one elementary surface on the ground with $\dot{F}(\vec{r}) = 1$.

The received information signal combines with internal noise $n(t)$. The resulting signals for subsequent processing take the following form

$$u(t) = s_r(t) + n(t). \tag{11}$$

For the given deterministic complex reflection coefficient model, optimal signal processing (10) is typically implemented through evaluation of the correlation integral

$$\dot{Y}(\vec{r}) = \int_0^T u(t)\dot{s}_0(t,\vec{r})d\vec{r}, \tag{12}$$

where T is the time of elementary surface on the ground observation.

In the case of noise absence, the physical meaning of complex scattering coefficient estimation can be described as

$$\widehat{\dot{F}}(\vec{r}) = \frac{1}{2}\int_D \dot{F}(\vec{r}_1)\dot{\Psi}(\vec{r}_1,\vec{r})d\vec{r}_1 = \frac{1}{2}\int_D \dot{\Psi}(\vec{r}_1,\vec{r})d\dot{Q}(\vec{r}_1), \tag{13}$$

where $\dot{\Psi}(\vec{r}_1,\vec{r})$ is the ambiguity function of SAR system, $\hat{\cdot}$is the sign of estimation.

When the individual signals within these integrals represent the impulse responses of filters, the operations (11) constitute matched filtering operations (matched to the reference signal), and the corresponding filters are referred to as matched filters. These operations enable coherent signal integration along the aircraft flight path and implement classical aperture synthesis, i.e. the creation of an artificial antenna aperture along the flight trajectory.

Signal processing according to (11) is optimal only in the case of deterministic model of the scattered coefficient $d\dot{Q}(\vec{r})$. But in real remote sensing measurements is not true. Scattering of the environment surfaces can be described as rough surface scattering, volume scattering, double bounce scattering.

Because of coherent processing and significant phase modulation of he scattered signal radar images of the underlying surfaces have spotted structure, named speckle noise [17, 18]. Example of such image from the radar imagery satellite Sentinel-1 is shown in the Figure 1. In this case, the image exhibits a well-defined speckle pattern, making it unclear what should be considered the actual image content and which elements are useful versus interference. The width of an individual speckle in the image roughly matches the width of the SAR ambiguity function in both azimuth and range directions [19, 20, 21, 22].

To mitigate the impact of speckle noise when estimating the complex scattering coefficient $\widehat{\dot{F}}(\vec{r})$, the squared modulus is computed and then smoothed using various linear and nonlinear filters [23, 24]. If we treat the complex scattering coefficient as a random variable, then this post-processing yields its statistical property in the form of variance

$$\overset{\sigma^{0}{}^{0}}{\sigma} \wedge(\vec{r}) = \left\langle \left|\widehat{\dot{F}}(\vec{r})\right|^2 \right\rangle = \left\langle \left[\left(Re\widehat{\dot{F}}(\vec{r})\right)^2 + \left(Im\widehat{\dot{F}}(\vec{r})\right)^2\right] \right\rangle, \tag{14}$$

where $\overset{\sigma^{0}{}^{0}}{\sigma} \wedge(\vec{r})$ is called radar cross section in radar measurements, $\langle\cdot\rangle$ is the sign of statistical averaging.

Based on the analysis of the scattering mechanism and coherent phase-accurate processing of real radar images, we can conclude that the scattering coefficient behaves as a random spatial process with an extremely narrow correlation function that is significantly narrower than the ambiguity function. There is no practical value in estimating the complex scattering coefficient itself. Instead, the focus should be on estimating its statistical property (13). The currently employed processing methods are suboptimal, as they were derived under different problem conditions. Optimizing the restoration of the function $\sigma^0(\vec{r})$ will require developing a modified aperture synthesis algorithm that accounts for the correlation properties of stochastic processes.

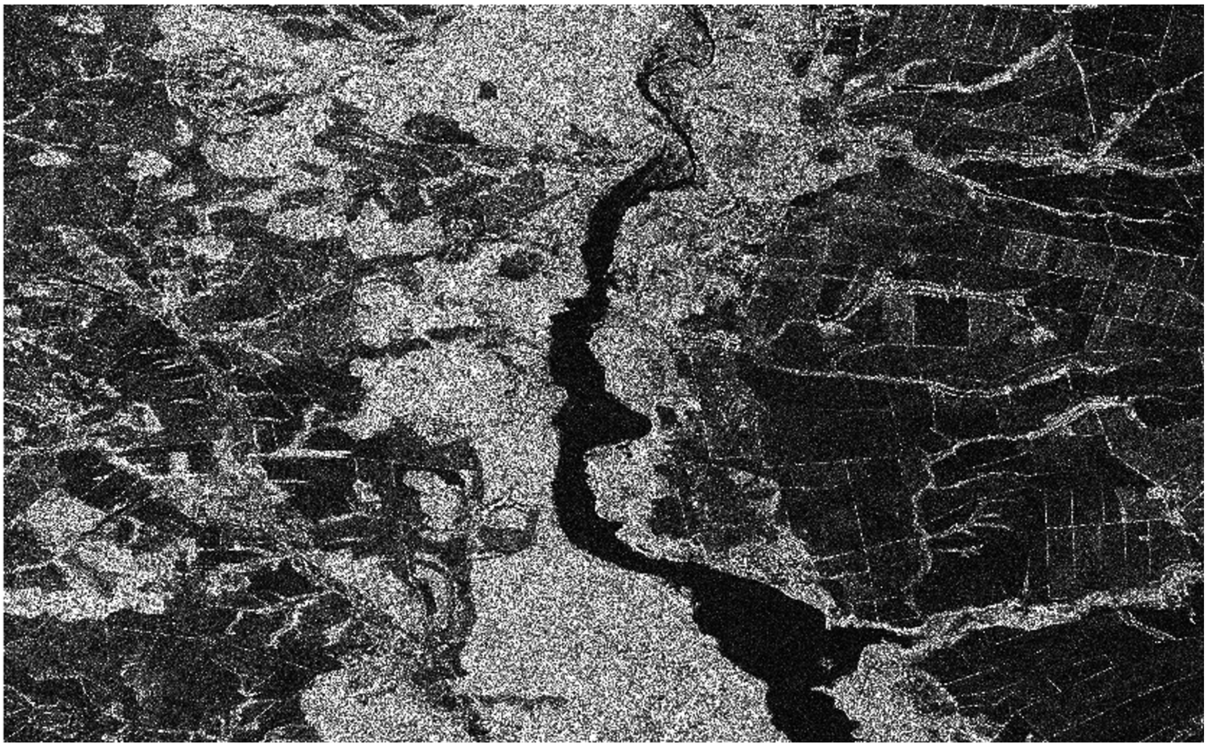

Figure 1: Radar image captured with satellite Sentinel-1.

3. Statistical optimization of radar imaging algorithm

The optimal approach for radar imaging of the Earth's surface will be derived using the maximum likelihood estimation framework [25, 26, 27].

For the case of a stochastic reflection coefficient, the correlation function of the observation equation (10) takes the form:

$$R_u(t_1, t_2) = \langle u(t_1)u(t_2)\rangle = \frac{1}{2}Re\int_{-\infty}^{\infty} \sigma^0(\vec{r})\dot{S}_0(t_1, \vec{r})\dot{S}_0^*(t_2, \vec{r})d\vec{r} + \frac{1}{2}N_{0n}\delta(t_1 - t_2), \tag{15}$$

where we suppose

$$\left\langle \dot{F}(\vec{r}_1)\dot{F}(\vec{r}_2) \right\rangle = \sigma^0(\vec{r}_1)\delta(\vec{r}_1 - \vec{r}_2) \tag{16}$$

is corelation function of $\dot{F}(\vec{r})$,

$$\langle n(t_1)n(t_2)\rangle = 0,5N_{0n}\delta(t_1 - t_2) \tag{17}$$

is corelation function of $n(t)$, N_{0n} is the internal noise power spectral density, $\dot{S}_0(t, \vec{r})$ is the complex envelope of $\dot{s}_0(t, \vec{r})$.

Assuming a zero-mean Gaussian random process $u(t)$, the likelihood functional for parameter $\sigma^0(\vec{r})$ takes the form

$$p[u(t)|\sigma^0(\vec{r})] = [0(r)]exp - 120T0Tu(t1)Wut1, t2, 0(x, y)u(t2)dt1dt2, \tag{18}$$

where $\kappa[\sigma^0(\vec{r})]$ is the constant that depend on parameter $\sigma^0(\vec{r}), W_u\left[t_1, t_2, \sigma^0(x, y)\right]$ represents the inverse correlation function, obtained by solving the integral equation

$$\int_0^T W_u\left[t_1, t_2, \sigma^0(\vec{r})\right] R_u\left[t_2, t_3, \sigma^0(\vec{r})\right] dt_2 = \delta(t_1 - t_3). \tag{19}$$

The desired parameter $\sigma^0(\vec{r})$ representing radar image does not appear directly in the observation equation as in classical SAR. Rather, it is embedded within the correlation and inverse correlation functions. Since $\sigma^0(\vec{r})$ is a coordinate-dependent function $\vec{r}$, the optimization problem for maximizing the likelihood functional (17) must be solved using variational methods. By computing the first variational derivative of functional (17) with respect to $\sigma^0(\vec{r})$ and setting it to zero, we obtain the following integral equation:

$$-\int_0^T\int_0^T \frac{\delta R_u\left[t_1,t_2,\sigma^0(\vec{r})\right]}{\delta\sigma^0(\vec{r})} W_u\left[t_1,t_2,\sigma^0(\vec{r})\right]dt_1dt_2 = \int_0^T\int_0^T u(t_1)\frac{\delta W_u\left[t_1,t_2,\sigma^0(\vec{r})\right]}{\delta\sigma^0(\vec{r})}u(t_2)dt_1dt_2. \tag{20}$$

The variational derivative of the inverse correlation function can be expressed as

$$\frac{\delta W_u\left[t_1,t_2,\sigma^0(\vec{r})\right]}{\delta\sigma^0(\vec{r})} = -\int_0^T\int_0^T W_u\left[t_1,t_3,\sigma^0(\vec{r})\right]\frac{\delta R_u\left[t_3,t_4,\sigma^0(\vec{r})\right]}{\delta\sigma^0(\vec{r})}W_u\left[t_4,t_2,\sigma^0(\vec{r})\right]dt_3dt_4. \tag{21}$$

The inverse correlation function has the form

$$W_u\left[t_1,t_2,\sigma^0(\vec{r})\right] = \int_0^T\int_0^T W_u\left[t_1,t_3,\sigma^0(\vec{r})\right]R_u\left[t_3,t_4,\sigma^0(\vec{r})\right]W_u\left[t_4,t_2,\sigma^0(\vec{r})\right]dt_3dt_4. \tag{22}$$

After substituting all components, equality (19) takes the following form:

$$\left\langle\left|\dot{Y}(\vec{r})\right|^2\right\rangle = \frac{1}{2}\int_{-\infty}^{\infty}\sigma^0(\vec{r}_1)\left|\dot{\Psi}_W(\vec{r},\vec{r}_1)\right|^2 d\vec{r}_1 + N_{0n}E_W(\vec{r}), \tag{23}$$

where

$$\dot{Y}(\vec{r}) = \int_0^T u(t_1)\dot{s}_{0W}\left[t_1,\sigma^0(\vec{r})\right]dt_1, \tag{24}$$

is the correlation integral of $\sigma^0(\vec{r})$ estimation,

$$\dot{s}_{0W}\left[t_1,\sigma^0(\vec{r})\right] = \int_0^T W_u\left[t_1,t_3,\sigma^0(\vec{r})\right]\dot{s}_0(t_3,\vec{r})dt_3 \tag{25}$$

is the reference signal for $\sigma^0(\vec{r})$ estimation,

$$E_W(\vec{r}) = \frac{1}{2}\int_0^T\left|\dot{s}_{0W}\left[t_3,\sigma^0(\vec{r})\right]\right|^2 dt_3 \tag{26}$$

is the energy of the reference signal,

$$\dot{\Psi}_W(\vec{r},\vec{r}_1) = \int_0^T \dot{s}_0(t_1,\vec{r})\dot{s}^*_{0W}(t_1,\vec{r})dt_1 \tag{27}$$

is the ambiguity function of SAR system recovering $\sigma^0(\vec{r})$. The left part of (22) is the optimal spatio-temporal signal processing algorithm and the right part is physical description of radar imaging with derived formulas.

Unlike previously mentioned solutions (11) the proposed signal processing method incorporates a decorrelation operation in the filter with pulse response $W_u\left[t_1,t_3,\sigma^0(\vec{r})\right]$, thereby increasing the number of statistically independent samples in the observed response. Furthermore, the operations of squared modulus formation and statistical averaging emerge naturally from the optimization solution rather than being introduced empirically.

The imaging process physically represents a convolution of the true image with the squared magnitude of the system's ambiguity function. Note that the convolution result is additionally offset by a systematic displacement $N_{0n}E_W(\vec{r})$.

4. Evaluation novel optimal processing algorithm

To verify the functionality of the proposed algorithm, it is necessary to perform simulation modelling of radar images. Based on the correlation function defined in equation (15), the complex scattering coefficient in the model should be represented as white Gaussian noise. However, this process is unrealizable in digital simulations due to its infinite variance and the need for infinitely dense sampling over any finite interval. To overcome this contradiction, we will represent the differential in integral (9) as a measure of the set of the stochastic Ito integral sum

$$\Delta\dot{Q}\left(\vec{r}_i\right) = \int_{\vec{r}_i}^{\vec{r}_i+\Delta\vec{r}} \dot{F}\left(\vec{\rho}\right) d\vec{\rho}. \tag{28}$$

On infinitesimal intervals $\Delta\vec{r}$ within the neighborhood of the variable's values $\vec{r}_i$ we consider discrete samples of the coherent image as their associated stochastic measures

$$\dot{F}(\vec{r}_i) = \frac{\Delta\dot{Q}\left(\vec{r}_i\right)}{\Delta\vec{r}} = \frac{1}{\Delta\vec{r}}\int_{\vec{r}_i}^{\vec{r}_i+\Delta\vec{r}} \dot{F}\left(\vec{\rho}\right) d\vec{\rho} = \frac{1}{\Delta\vec{r}}\int_{\vec{r}_i}^{\vec{r}_i+\Delta\vec{r}} Re\dot{F}\left(\vec{\rho}\right) d\vec{\rho} + \frac{1}{\Delta\vec{r}}\int_{\vec{r}_i}^{\vec{r}_i+\Delta\vec{r}} Im\dot{F}\left(\vec{\rho}\right) d\vec{\rho}, \tag{29}$$

where $\Delta\vec{r}$ denotes the standard measure of the sampling interval, equivalent to its area $\Delta\mathrm{x}\Delta\mathrm{y}$.

Following the classical mean value theorem of mathematical analysis, these samples represent the $\dot{F}(\vec{r})$ average values over their respective sampling intervals $\Delta\vec{r}$. The resulting random increments $\Delta\dot{Q}\left(\vec{r}_i\right)$ and complex numbers $\dot{F}(\vec{r}_i)$ will be statistically independent with zero mean, forming discretized analogues of a true coherent image $\dot{F}(\vec{r})$. Such sequences of independent zero-mean random variables are conventionally referred to as discrete white Gaussian noise [28, 29].

Variance of (28) has the following form

$$\sigma_F^2\left(\vec{r}_i\right) = \left\langle \left| \frac{1}{\Delta\vec{r}}\int_{\vec{r}_i}^{\vec{r}_i+\Delta\vec{r}} \dot{F}\left(\vec{\rho}\right) d\vec{\rho} \right|^2 \right\rangle = \frac{1}{(\Delta\vec{r})^2}\int_{\vec{r}_i}^{\vec{r}_i+\Delta\vec{r}}\int_{\vec{r}_i}^{\vec{r}_i+\Delta\vec{r}} \left\langle \dot{F}\left(\vec{\rho}_1\right)\dot{F}^*\left(\vec{\rho}_2\right)\right\rangle d\vec{\rho}_1 d\vec{\rho}_2 = \frac{\sigma^0\left(\vec{r}_i\right)}{\Delta\vec{r}}, \tag{30}$$

The variance distribution of the ideal incoherent radar image is shown in Figure 2. Figure 3 represents plots of the statistically independent components of the discrete complex reflection coefficient $\frac{1}{\Delta\vec{r}}\int_{\vec{r}_i}^{\vec{r}_i+\Delta\vec{r}} Re\dot{F}\left(\vec{\rho}\right) d\vec{\rho} and \frac{1}{\Delta\vec{r}}\int_{\vec{r}_i}^{\vec{r}_i+\Delta\vec{r}} Im\dot{F}\left(\vec{\rho}\right) d\vec{\rho}$. Figure 4 displays the resulting radar image generated using algorithm (11) with following operations of squared modulus and averaging. For comparison, Figure 5 presents the radio image obtained through the optimal radar cross section estimation algorithm (22).

To quantify performance, we employed standardized image quality metrics for comparison with reference data [30, 31, 32, 33, 34]. Table 1 presents both the metric definitions and their corresponding values, demonstrating the quality assessment of radio images produced by both conventional and our proposed optimal methods.

Analysis of Table 1 reveals that decorrelation processing yields superior performance across most quality metrics. This improvement occurs because the decorrelation filter approximates the received signal as white noise, particularly at high signal-to-noise conditions. The filter reduces speckle size in the primary radar image while increasing speckle density within the secondary processing window. This higher speckle count enhances averaging effectiveness, ultimately improving radar image resolution as measured by the effective scattering surface representation.

5. Conclusions

This study presents a novel approach to optimizing synthetic aperture radar (SAR) signal processing by addressing the stochastic nature of surface reflections, which significantly enhances radar imaging performance. By modeling the complex scattering coefficient as a random spatial process it is developed a statistically optimized algorithm for azimuth and range compression processing. The proposed method

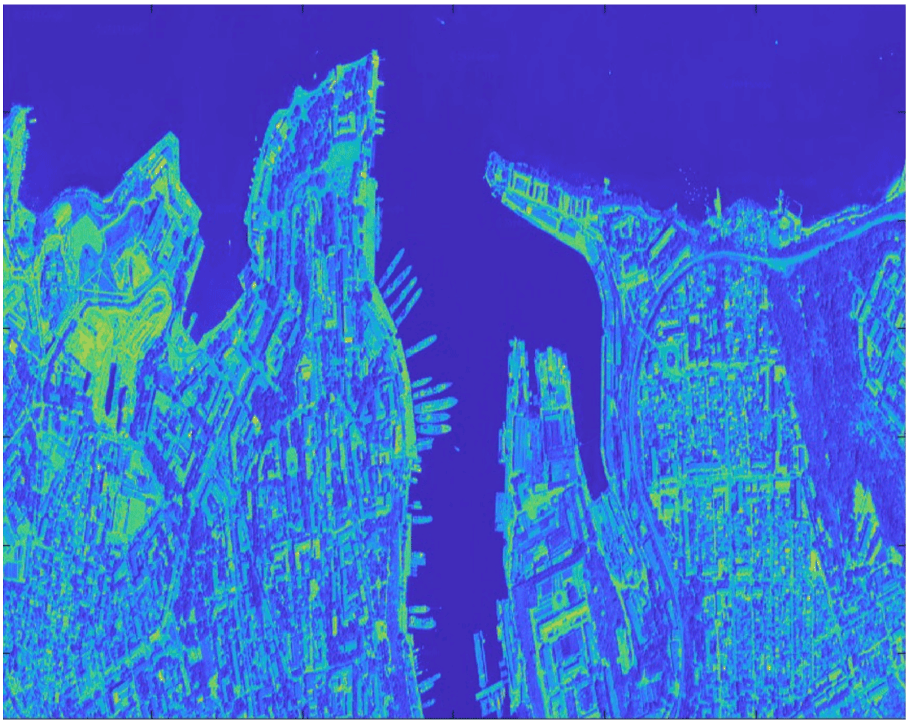

Figure 2: Ideal radar cross section.

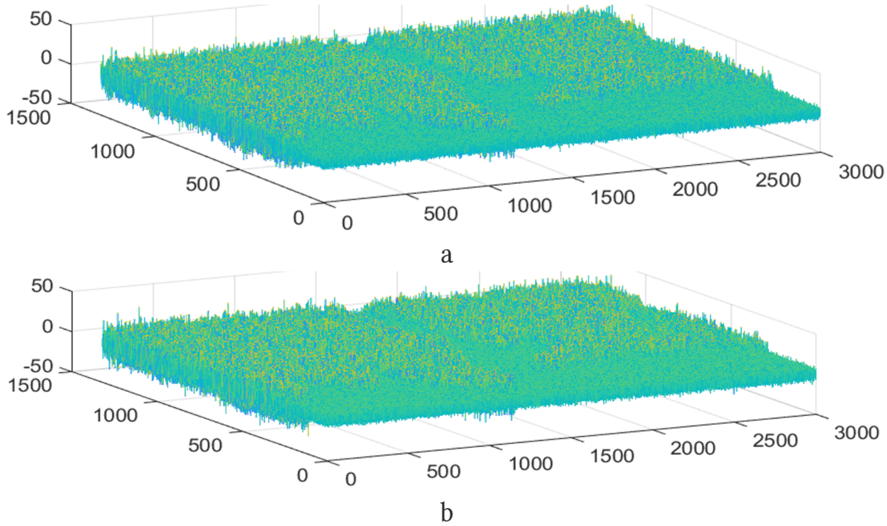

Figure 3: Components of the discrete complex reflection coefficient: a – real part, b – imaginary part.

incorporates a decorrelation operation within the signal processing framework, which increases the number of statistically independent samples, mitigates speckle noise, and improves image quality without relying on empirical post-processing techniques.

Simulation results demonstrate that the modified algorithm outperforms conventional SAR processing methods across multiple standardized image quality metrics. The decorrelation filter approximates the received signal as white noise under high signal-to-noise conditions, reducing speckle size and increasing speckle density, which enhances the effectiveness of averaging and improves the resolution of the radar cross section representation.

Future work could focus on refining the algorithm for real-time implementation, exploring its applicability to multi-polarization SAR systems, and validating its performance with diverse datasets

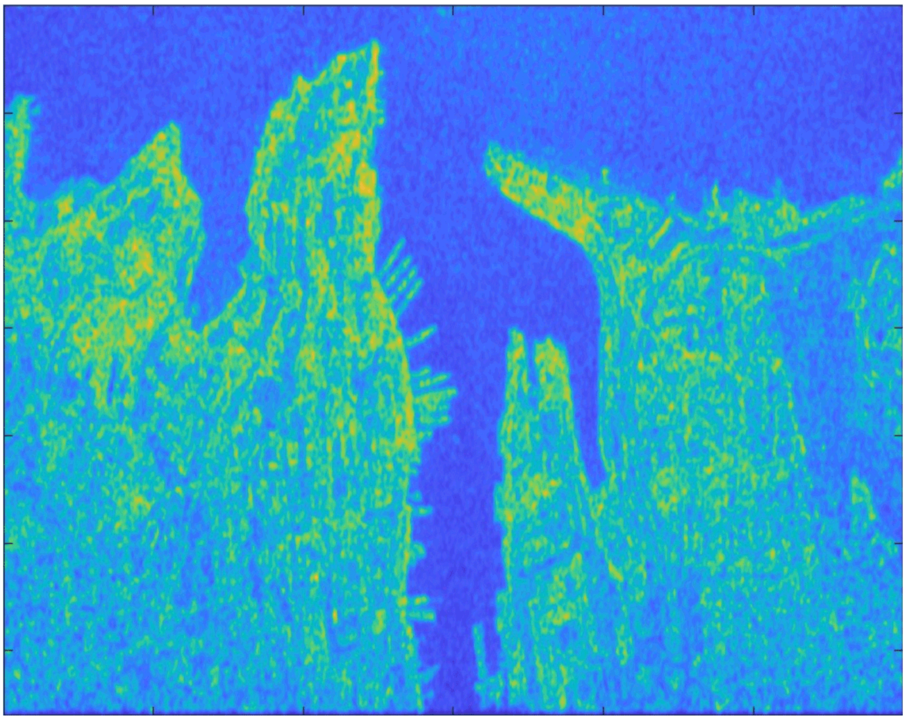

Figure 4: Estimation of radar cross section with algorithm (11).

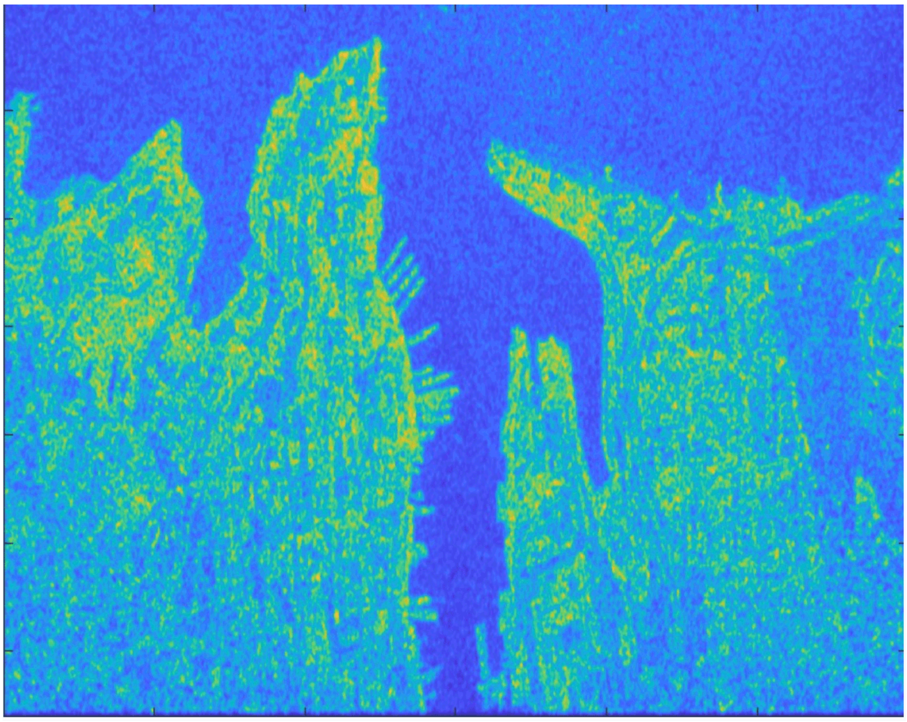

Figure 5: Estimation of radar cross section with modified algorithm (22).

from operational SAR platforms. This advancement contributes to the broader field of remote sensing by providing a more accurate and reliable method for high-resolution imaging under challenging environmental conditions.

Table 1
Quality evaluation of the classical and novel radar imaging algorithms.

Metric	Ideal radar cross section	Classical radar imaging	Modified radar imaging
Average Difference	0	16.0394	16.3491
Feature Similarity Extended	1	0.3860	0.4673
Structural Similarity Index	1	0.5638	0.6262
Normalized cross-correlation	1	0.9887	0.9893
Noise Quality Measure		13.6155	13.6268
Peak Signal-to-Noise Ratio	99	19.0089	19.2281
Mean square error	0	816.9412	776.7219
Structural Content	1	0.9016	0.9015
SVD-Based Image Quality Measure	0	22.1278	22.4622
Visual Information Fidelity	1	0.2476	0.2541

6. Acknowledgments

The work has been funded by the Ministry of Education and Science of Ukraine. The state registration number of the projects are 0123U102002 and 0123U102000.

Declaration on Generative AI

The author(s) have not employed any Generative AI tools.

References

[1] M. Inggs, Synthetic aperture radar during the 50 years of the aerospace and electronic systems society, IEEE Aerospace and Electronic Systems Magazine 38 (2023) 22–31. doi:10.1109/MAES.2022.3216263.

[2] Z. Sjanic, F. Gustafsson, Simultaneous navigation and synthetic aperture radar focusing, IEEE Transactions on Aerospace and Electronic Systems 51 (2015) 1253–1266. doi:10.1109/TAES.2015.120820.

[3] H. Sun, M. Shimada, F. Xu, Recent advances in synthetic aperture radar remote sensing—systems, data processing, and applications, IEEE Geoscience and Remote Sensing Letters 14 (2017) 2013–2016. doi:10.1109/LGRS.2017.2747602.

[4] Y. Deng, W. Yu, P. Wang, D. Xiao, W. Wang, K. Liu, H. Zhang, The high-resolution synthetic aperture radar system and signal processing techniques: Current progress and future prospects [review papers], IEEE Geoscience and Remote Sensing Magazine 12 (2024) 169–189. doi:10.1109/MGRS.2024.3456444.

[5] X. Chen, Z. Dong, Z. Zhang, C. Tu, T. Yi, Z. He, Very high resolution synthetic aperture radar systems and imaging: A review, IEEE Journal of Selected Topics in Applied Earth Observations and Remote Sensing 17 (2024) 7104–7123. doi:10.1109/JSTARS.2024.3374429.

[6] R. Bürgmann, P. A. Rosen, E. J. Fielding, Synthetic aperture radar interferometry to measure earth's surface topography and its deformation, Annual Review of Earth and Planetary Sciences 28 (2000) 169–209. URL: https://www.annualreviews.org/content/journals/10.1146/annurev.earth.28.1.169. doi:https://doi.org/10.1146/annurev.earth.28.1.169.

[7] A. Nambiar, A. Vaigandla, S. Rajendran, Efficient ship detection in synthetic aperture radar images and lateral images using deep learning techniques, in: OCEANS 2022, Hampton Roads, 2022, pp. 1–10. doi:10.1109/OCEANS47191.2022.9977152.

[8] V. Pavlikov, V. Volosyuk, S. Zhyla, H. N. Van, K. N. Van, A new method of multi-frequency active aperture synthesis for imaging of sar blind zone under aerospace vehicle, in: 2017 14th International

Conference The Experience of Designing and Application of CAD Systems in Microelectronics (CADSM), 2017, pp. 118–120. doi:10.1109/CADSM.2017.7916099.
[9] T. Nikitina, B. Kuznetsov, Y. Averyanova, O. Sushchenko, I. Ostroumov, N. Kuzmenko, et al., Method for design of magnetic field active silencing system based on robust meta model, in: S. Shukla, H. Sayama, J. V. Kureethara, D. K. Mishra (Eds.), Data Science and Security. IDSCS 2023. Lecture Notes in Networks and Systems, vol. 922, Springer Nature Singapore, Singapore, 2024, pp. 103–111. doi:10.1007/978-981-97-0975-5_9.
[10] A. Popov, E. Tserne, V. Volosyuk, S. Zhyla, V. Pavlikov, N. Ruzhentsev, et al., Invariant polarization signatures for recognition of hydrometeors by airborne weather radars, in: O. Gervasi, B. Murgante, D. Taniar, B. O. Apduhan, A. C. Braga, C. Garau, A. Stratigea (Eds.), Computational Science and Its Applications – ICCSA 2023. ICCSA 2023. Lecture Notes in Computer Science, vol. 13956, Springer Nature Switzerland, Cham, 2023, pp. 201–217. doi:10.1007/978-3-031-36805-9_14.
[11] V. V. Pavlikov, V. K. Volosyuk, S. S. Zhyla, N. Van Huu, Active aperture synthesis radar for high spatial resolution imaging, in: 2018 9th International Conference on Ultrawideband and Ultrashort Impulse Signals (UWBUSIS), 2018, pp. 252–255. doi:10.1109/UWBUSIS.2018.8520021.
[12] V. K. Volosyuk, V. V. Pavlikov, S. S. Zhyla, Phenomenological description of the electromagnetic field and coherent images in radio engineering and optical systems, in: 2018 IEEE 17th International Conference on Mathematical Methods in Electromagnetic Theory (MMET), 2018, pp. 302–305. doi:10.1109/MMET.2018.8460321.
[13] V. K. Volosyuk, S. Zhila, D. Kolesnikov, Phenomenological description of coherent radar images based on the concepts of the measure of set and stochastic integral, Telecommunications and Radio Engineering 78 (2019).
[14] V. Volosyuk, S. Zhyla, D. Vlasenko, O. Inkarbaieva, D. Kolesnikov, G. Cherepnin, Concepts of primary and secondary coherent images in radar and optical systems, in: 2022 IEEE 3rd International Conference on System Analysis Intelligent Computing (SAIC), 2022, pp. 1–6. doi:10.1109/SAIC57818.2022.9923005.
[15] SAR, Synthetic aperture radar (sar), 2025. URL: https://www.earthdata.nasa.gov/learn/earth-observation-data-basics/sar.
[16] M. Ottinger, C. Kuenzer, Spaceborne l-band synthetic aperture radar data for geoscientific analyses in coastal land applications: A review, Remote Sensing 12 (2020). URL: https://www.mdpi.com/2072-4292/12/14/2228. doi:10.3390/rs12142228.
[17] J.-S. Lee, Speckle analysis and smoothing of synthetic aperture radar images, Computer Graphics and Image Processing 17 (1981) 24–32. URL: https://www.sciencedirect.com/science/article/pii/S0146664X81800056. doi:https://doi.org/10.1016/S0146-664X(81)80005-6.
[18] T. Nikitina, B. Kuznetsov, N. Ruzhentsev, O. Havrylenko, K. Dergachov, V. Volosyuk, et al., Algorithm of robust control for multi-stand rolling mill strip based on stochastic multi-swarm multi-agent optimization, in: S. Shukla, H. Sayama, J. V. Kureethara, D. K. Mishra (Eds.), Data Science and Security. IDSCS 2023. Lecture Notes in Networks and Systems, vol. 922, Springer Nature Singapore, Singapore, 2024, pp. 247–255. doi:10.1007/978-981-97-0975-5_22.
[19] V. Bhola, T. Sharma, J. Bhatnagar, Image quality assessment techniques, Int. J. Adv. Res. Comput. Sci. Softw. Eng (2014) 156–161.
[20] D. Ngo, S. Lee, Q.-H. Nguyen, T. M. Ngo, G.-D. Lee, B. Kang, Single image haze removal from image enhancement perspective for real-time vision-based systems, Sensors 20 (2020). URL: https://www.mdpi.com/1424-8220/20/18/5170. doi:10.3390/s20185170.
[21] Z. Wang, A. Bovik, H. Sheikh, E. Simoncelli, Image quality assessment: from error visibility to structural similarity, IEEE Transactions on Image Processing 13 (2004) 600–612. doi:10.1109/TIP.2003.819861.
[22] F. Zhao, Q. Huang, W. Gao, Image matching by normalized cross-correlation, in: 2006 IEEE International Conference on Acoustics Speech and Signal Processing Proceedings, volume 2, 2006, pp. II–II. doi:10.1109/ICASSP.2006.1660446.
[23] L. Zhang, H. Wang, L. Wang, C. Pan, C. Huo, Q. Liu, X. Wang, Filtered convolution for synthetic aperture radar images ship detection, Remote Sensing 14 (2022). URL: https://www.mdpi.com/

2072-4292/14/20/5257. doi:10.3390/rs14205257.
[24] R. K. Painam, S. Manikandan, A comprehensive review of sar image filtering techniques: systematic survey and future directions, Arabian Journal of Geosciences 14 (2021) 37.
[25] B. Tang, J. Tang, Y. Zhang, Z. Zheng, Maximum likelihood estimation of dod and doa for bistatic mimo radar, Signal Processing 93 (2013) 1349–1357. URL: https://www.sciencedirect.com/science/article/pii/S0165168412004069. doi:https://doi.org/10.1016/j.sigpro.2012.11.011.
[26] J. Pan, Modified maximum likelihood space registration method for shipborne multi-radar signal processing, Journal of Engineering Research 13 (2025) 185–197. URL: https://www.sciencedirect.com/science/article/pii/S2307187723002602. doi:https://doi.org/10.1016/j.jer.2023.09.035.
[27] K. Tan, W. Li, Q. Zhang, Y. Huang, J. Wu, J. Yang, Penalized maximum likelihood angular super-resolution method for scanning radar forward-looking imaging, Sensors 18 (2018). URL: https://www.mdpi.com/1424-8220/18/3/912. doi:10.3390/s18030912.
[28] F. K. Jondral, White gaussian noise – models for engineers, Frequenz 72 (2018) 293–299. URL: https://doi.org/10.1515/freq-2017-0064. doi:doi:10.1515/freq-2017-0064.
[29] S. Zhao, Y. S. Shmaliy, F. Liu, Fast computation of discrete optimal fir estimates in white gaussian noise, IEEE Signal Processing Letters 22 (2015) 718–722. doi:10.1109/LSP.2014.2368777.
[30] R. de Freitas Zampolo, R. Seara, A comparison of image quality metric performances under practical conditions, in: IEEE International Conference on Image Processing 2005, volume 3, 2005, pp. III–1192. doi:10.1109/ICIP.2005.1530611.
[31] K. Kordov, S. Zhelezov, Steganography in color images with random order of pixel selection and encrypted text message embedding, PeerJ Computer Science 7 (2021) e380.
[32] S. Sanjith, R. Ganesan, Overview of image quality metrics with perspective to satellite image compression, International Journal of Engineering Research in Africa 24 (2016) 112–123. doi:10.4028/www.scientific.net/JERA.24.112.
[33] A. Shnayderman, A. M. Eskicioglu, Evaluating the visual quality of watermarked images, in: E. J. D. III, P. W. Wong (Eds.), Security, Steganography, and Watermarking of Multimedia Contents VIII, volume 6072, International Society for Optics and Photonics, SPIE, 2006, p. 607222. URL: https://doi.org/10.1117/12.641972. doi:10.1117/12.641972.
[34] S. Rezazadeh, S. Coulombe, Low-complexity computation of visual information fidelity in the discrete wavelet domain, in: 2010 IEEE International Conference on Acoustics, Speech and Signal Processing, 2010, pp. 2438–2441. doi:10.1109/ICASSP.2010.5496298.